The Astrophysical Journal, 656:980–990, 2007 February 20

MODELING *SPITZER* OBSERVATIONS OF VV SER. I. THE CIRCUMSTELLAR DISK OF A UX ORIONIS STAR

Klaus M. Pontoppidan,[1,2,3] Cornelis P. Dullemond,[4] Geoffrey A. Blake,[1] A. C. Adwin Boogert,[1]
Ewine F. van Dishoeck,[2] Neal J. Evans II,[5] Jacqueline Kessler-Silacci,[5] and and Fred Lahuis[2]
Received 2005 September 12; accepted 2006 September 29

ABSTRACT

We present mid-infrared *Spitzer* IRS spectra of the UX Orionis star VV Ser, combined with interferometric and spectroscopic data from the literature covering UV to submillimeter wavelengths. The full set of data are modeled by an axisymmetric Monte Carlo radiative transfer code to test the prediction of Dullemond et al. that disks around UX Orionis stars are self-shadowed and seen nearly edge-on. Our model is consistent with all the available observational constraints, providing strong support for this interpretation. The mid-infrared SED is declining and exhibits weak silicate emission features, consistent with a self-shadowed geometry. MIPS imaging shows that the disk has a small grain dust mass as low as $0.8 \times 10^{-7}\ M_{\odot}$, which may be due to strong grain growth and settling. The grains in the upper layers of the puffed-up inner rim must be small (0.01–0.4 μm) to reproduce the colors ($R_V \sim 3.6$) of the optical light curve, while the silicate emission features indicate that grains in the outer disk (>1–2 AU) are somewhat larger (0.3–3.0 μm). If grains in the inner disk are small, the location of the puffed-up inner rim is estimated to be at 0.7–0.8 AU. This is almost twice the rim radius estimated from near-infrared interferometry. Since larger (more gray) grains are able to penetrate closer to the star for the same dust sublimation temperature, we suggest a model in which large grains in the disk midplane reach to within 0.25 AU of the star, while small grains in the disk surface create a puffed-up rim at ~0.7–0.8 AU.

Subject headings: accretion, accretion disks — circumstellar matter — infrared: stars — stars: formation — stars: pre–main-sequence

Online material: color figures

1. INTRODUCTION

Edge-on and nearly edge-on disks around Herbig Ae and T Tauri stars are ideal objects for studying the structure and composition of protoplanetary disks. In addition to infrared emission from the disk, one has supplemental information from absorption of starlight along the line of sight through the surface layers or the interior of the disk. This probing technique has been used by various authors to analyze the dust size distribution in such disks (Wood et al. 2002; Duchêne et al. 2003; Wolf et al. 2003; Watson & Stapelfeldt 2004) and to determine the abundance of icy grain in the outer regions of these disks (Thi et al. 2002; Pontoppidan et al. 2005).

Because of the additional constraints compared with other disks, it is clear that edge-on disks are ideal targets for detailed studies involving spectroscopy and images at many wavelengths. Given the many new sensitive observational facilities, including space-based mid-infrared imaging and spectroscopy as well as near-infrared interferometry, a powerful approach to analyzing these data is the simultaneous fitting with a multidimensional continuum radiative transfer model of the disk.

A particularly interesting subclass of (presumably) nearly edge-on disks is "UX Orionis stars." For these objects the stellar flux on average is only marginally extincted, but they undergo frequent, highly nonperiodic extinction events, lasting a few days to weeks, in which the star dims strongly and becomes redder. A model in which dusty clumps in Keplerian orbits temporarily obscure the central star, as originally proposed by Grinin (1988) seems the best explanation for the observational constraints. In particular, in the bottom of very deep minima, the color track eventually turns around and the colors become bluer. In the context of the "dust clump" model, this characteristic "blueing" in deep minima signifies that the stellar photosphere has disappeared entirely from view and that scattered light from the disk surface begins to dominate in the optical wave bands.

While it has been suggested that these extinction events may be due to comets passing in front of the star (Grady et al. 1997), others have argued for a nearly edge-on disk scenario in which one narrowly looks over the surface of the disk toward the star, where small hydrodynamic perturbations temporarily pass through the line of sight (Bertout 2000; Natta & Whitney 2000). The short timescales for these extinction events indicate that the perturbations should happen close to the dust evaporation radius. It was argued by Natta et al. (2001) and Dullemond et al. (2003) that the puffed-up inner rim of the dusty part of the disk (see also Dullemond et al. 2001) is likely to be the location where these extinction events are produced. The inclination of the disk is such that the line of sight passes just over (or just through) the upper edge of the puffed-up inner rim, and hydrodynamic fluctuations can then vary the extinction of starlight along the line of sight on a timescale consistent with what is observed. Since the central star is typically not strongly attenuated outside a UX Orionis event, this scenario works only if the line of sight does not pass through many magnitudes of extinction in the outer regions of the disk. Hence, the outer parts of the disk cannot have a flaring geometry for these sources.

The conclusion reached by Dullemond et al. (2003) was that all UX Orionis stars should be self-shadowed disks, in which the outer disk is geometrically thin enough to lie entirely in the shadow cast by the puffed-up inner rim, and therefore does not intersect a line of sight passing just over the edge of this rim. A marginal flaring, in which the outer disk just barely appears above the inner-rim shadow, may be possible as well, as long as the resulting extinction along the line of sight is marginal.

[1] California Institute of Technology, Division of Geological and Planetary Sciences, Pasadena, CA; pontoppi@gps.caltech.edu.
[2] Leiden Observatory, Leiden, Netherlands.
[3] Hubble Fellow.
[4] Max-Planck-Institut für Astronomie, Heidelberg, Germany.
[5] Department of Astronomy, University of Texas, Austin, TX.

It was shown by these authors that the shape of the spectral energy distributions of all known UX Orionis objects indeed indicate that they are mostly nonflared (self-shadowed) disks, with some exceptions lying just on the border between flaring and self-shadowing disks. This gives strong support for the "inclined disk" scenario.

As part of the *Spitzer Space Telescope* Legacy program "From Molecular Cores to Protoplanetary Disks" (c2d; Evans et al. 2003), we obtained 5.2–37.0 μm spectroscopy, as well as IRAC and MIPS images of the well-known UX Orionis star VV Ser. The star was originally singled out for further study due to the presence of an extended (over 4′) mid-infrared nebulosity surrounding it. This nebulosity is analyzed in detail in a companion paper (Pontoppidan et al. 2007, hereafter Paper II), in which it is argued that the nebulosity is due to the quantum heating of polycyclic aromatic hydrocarbons (PAHs) as well as very small silicate or carbon grains. Imprinted on the nebulosity is a wedge-like dark band, which we interpret as a shadow cast by a small (less than a few 100 AU) nearly edge-on disk (see also Pontoppidan & Dullemond 2005). The presence of a disk shadow allows a relatively accurate determination of the inclination and position angle of the system, which is crucial for the interpretation of VV Ser as a UX Orionis star.

In this paper we concentrate on analyzing VV Ser in terms of the UX Orionis phenomenon. To do this we create an axisymmetric radiative transfer model using a wide range of data to constrain the disk structure. This includes not only the *Spitzer* data, but also submillimeter images obtained using SCUBA on the James Clerk Maxwell Telescope (JCMT),[6] near-infrared interferometric visibilities and optical light curves from the literature. Although some aspects of an axisymmetric model cannot be uniquely constrained, we can make firm conclusions about the disk geometry, grain sizes, inner rim structure, etc. More importantly, our analysis gives further strong evidence in favor of the scenario for UX Orionis stars put forward by Dullemond et al. (2003). In doing so, this lends support for the puffed-up inner rim model of Natta et al. (2001) and Dullemond et al. (2001) as well as for the interpretation of the near-IR to far-IR slope of the SED in terms of flaring versus self-shadowed disks (Dullemond & Dominik 2004; Meeus et al. 2001). This scenario allows us to interpret all the observed data of VV Ser in terms of a disk model with a simple geometrical interpretation.

We construct an axisymmetric radiative transfer model of the entire system from 0.5 to 50,000 AU scales. The main objectives are to test the scenario in which the UX Ori phenomenon is caused by a nearly edge-on disk, whether a disk shadow can plausibly be projected into the mid-infrared PAH nebulosity (see Paper II) and finally to use the model to constrain the structure and dynamics of the puffed-up inner rim.

This method necessarily targets specific objects for detailed modeling, and one should take care when generalizing from one specific object to a class of disks. One central point to this study is to determine observable predictions that can be applied to other UX Orionis stars, or even protoplanetary disks in general.

In this paper we first describe the observations that have been collected (§ 2) and the characteristics of the source (§ 3). In § 4 the radiative transfer model is presented. Section 5 discusses how each observational constraint is implemented into the model as well as possible sources of degeneracies.

[6] The JCMT is operated by the Joint Astronomy Centre in Hilo, Hawaii, on behalf of the parent organizations: the Particle Physics and Astronomy Research Council in the United Kingdom, the National Research Council of Canada, and the Netherlands Organization for Scientific Research.

2. OBSERVATIONS

The primary constraints on the model of VV Ser are provided by mid-infrared spectroscopy and imaging obtained with the *Spitzer Space Telescope* (Werner et al. 2004). Mid-infrared spectra of VV Ser were obtained with the *Spitzer* Infrared Spectrometer (IRS; Houck et al. 2004) using the short-low (SL) module from 5.2–14.5 μm, the short-high (SH) module from 9.9–19.6 μm, and the long-high (LH) module from 19–37 μm. The spectra were reduced using the pipeline version S11.0.2 and extracted with the c2d extraction routines. The SL spectra were extracted in a 12 pixel aperture. The background was estimated using the entire length of the slit and subtracted using a high-order polynomial fit to the measured background in order to minimize any additional noise from the background subtraction. The SH and LH spectra were extracted using full aperture extractions. The short slits in the high-resolution modules cause any background subtraction to be highly PSF model dependent. Consequently, the background was not subtracted from the SH and LH spectra. Since VV Ser is a bright source between 10 and 40 μm, we estimate the background to be a minor contribution, even considering the extended emission present around the source (see Paper II). The orders and modules were matched by scaling to the shortest wavelength order. The scaling factors applied were 5%–10%, and the absolute flux level of the spectrum is therefore considered accurate only to 10%–20%. The spectrum of VV Ser has AOR Key 0005651200. We present IRAC and MIPS imaging at 3.6, 4.5, 5.6, 8.0, 24, and 70 μm of the area surrounding VV Ser in Paper II.

In support of the *Spitzer* observations, additional continuum data at 850 and 450 μm were obtained in service mode with SCUBA on the JCMT on 2005 January 27. VV Ser was observed in a 64-point jiggle map (2.3′ field) with approximately 1 hour of integration. The weather was good with 225 Gz sky opacities of about 0.05. The pointing was checked regularly and found to be accurate to within a few arcseconds. Maps of CRL2688 and Mars were used for calibration purposes. The absolute calibration is accurate to about $\pm$20%. The beam size (HPBW) of the SCUBA observations is approximately 14″ at 850 μm. No continuum emission was detected toward VV Ser with a 3 σ upper limit of 10 mJy beam^{-1}.

An ultraviolet spectrum obtained with the *International Ultraviolet Explorer* (*IUE*) was taken from MAST, the Multimission Archive at the Space Telescope Science Institute (STScI).[7] More than 12 years of photometric monitoring in the optical *UBVRI* bands was taken from the catalog of Rostopchina et al. (2001). The photometry for the VV Ser point source is summarized in Table 1.

3. SOURCE DESCRIPTION

VV Ser is a typical UX Orionis star located in the Serpens molecular cloud. The adopted distance of VV Ser is $\sim$260 pc as determined for the Serpens molecular complex by Straizys et al. (1996). There is some variation in the literature regarding the effective temperature of VV Ser, although most classify the star as a late-B type. Hernández et al. (2004) identify VV Ser as a B6 star due to the presence of a number of He lines in their low-resolution spectra. Mora et al. (2001) find a spectral type of A0 using high-resolution spectroscopy. The exact choice does have measurable consequences for the model SED at wavelengths below $\sim$1 μm.

[7] Some of the data presented in this paper were obtained from MAST, at STScI. STScI is operated by the Association of Universities for Research in Astronomy (AURA), Inc., under NASA contract NAS5-26555. Support for MAST for non-*HST* data is provided by the NASA Office of Space Science via grant NAG5-7584 and by other grants and contracts.

TABLE 1
PHOTOMETRY OF VV SER

Wavelength (μm)	Flux[a] (Jy)	References
0.2	$(4 \pm 2) \times 10^{-4}$	*IUE*
0.365	0.011 ± 0.0005	Rostopchina et al. (2001)
0.44	0.035 ± 0.002	Rostopchina et al. (2001)
0.55	0.077 ± 0.004	Rostopchina et al. (2001)
0.70	0.14 ± 0.007	Rostopchina et al. (2001)
0.90	0.28 ± 0.014	Rostopchina et al. (2001)
1.235	0.47 ± 0.02	2MASS
1.662	0.97 ± 0.05	2MASS
2.159	1.87 ± 0.09	2MASS
3.79	3.0 ± 0.1	Berrilli et al. (1992)
4.64	3.4 ± 0.2	Berrilli et al. (1992)
5.5	4.2 ± 0.1	*Spitzer* IRS, this paper
8.0	4.5 ± 0.1	*Spitzer* IRS, this paper
12.0	4.2 ± 0.2	*Spitzer* IRS, this paper
25.0	3.4 ± 0.2	*Spitzer* IRS, this paper
36.0	2.7 ± 0.2	*Spitzer* IRS, this paper
70.0	0.35 ± 0.1	*Spitzer* MIPS, Paper II
450	<0.18 (3 σ)	JCMT SCUBA, this paper
850	<0.03 (3 σ)	JCMT SCUBA, this paper

[a] The optical photometry is for the "quiescent" state.

The optical colors favor a star closer to A0 than B6. The stellar luminosity of 49 $L_\odot$ also suggests that VV Ser is of later type since a B6 classification puts it below the ZAMS in the HR diagram (Siess et al. 2000).

Since the optical-UV spectrum of VV Ser does not appear to be strongly veiled and is of high quality, it is possible to derive an accurate stellar luminosity of $(49 \pm 5) \times (d/260\ \mathrm{pc})^2\ L_\odot$. Using the evolutionary tracks of Siess et al. (2000) and an effective temperature of 10,200 K, this gives a stellar mass of $2.6 \pm 0.2\ M_\odot$ and an age of 3.5 ± 0.5 Myr for a solar metallicity. The uncertainties reflect the uncertainties in the luminosity and $T_{\rm eff}$ rather than those of the model tracks.

The optical colors of the star correspond to a steady extinction of $A_V \sim 3$, but with frequent, nonperiodical dips lasting of order 10 days with brightness minima corresponding to 0.5–4.0 mag of additional extinction.

4. MODEL

To model the observed SED and *Spitzer* imaging of VV Ser, we use the axisymmetric Monte Carlo radiative transfer code RADMC (Dullemond & Dominik 2004) in combination with the ray-tracer of the more general code RADICAL (Dullemond & Turolla 2000). The density structure is axisymmetric, but the photons are followed in all three dimensions. The code is used to derive the temperature structure of a given dust distribution. The dust temperature is determined for a passive disk, i.e., it is assumed that accretion heating is negligible relative to direct stellar irradiation. This is justified by the high luminosity of the central star (49 $L_\odot$), since the accretion luminosity is $\lesssim 3\ L_\odot$ for accretion rates $\dot{M} \lesssim 10^{-7}\ M_\odot\ \mathrm{yr}^{-1}$ (Kenyon et al. 1993). The low mass of the disk $[8 \times 10^{-6}\ M_\odot \times (R_{\rm gas\ to\ dust}/100)]$, where $R_{\rm gas\ to\ dust}$ is the gas to dust mass ratio (see § 5.1) also limits the possible range of accretion rates, since only a small fraction of the entire disk mass can be expected to accrete per year. The low mass of the disk is particularly well constrained by the 70 μm MIPS point as well as the upper limit to the 850 μm flux.

Once a temperature structure has been determined, RADICAL can be used to create SEDs and images. The code is restricted to isotropic scattering. Taking nonisotropic scattering into account may change the optical colors of the model somewhat, but without resolved optical images of the disk, nonisotropic scattering effects cannot be properly constrained. One advantage of the code is the ability to include an arbitrary number of dust components, each with a unique opacity. The setup has been used to model similar protostellar disks (Pontoppidan et al. 2005; Pontoppidan & Dullemond 2005), while the code itself has been extensively tested for other applications (van Bemmel & Dullemond 2003; Dullemond & Dominik 2005; Meijerink et al. 2005) and has recently been benchmarked relative to independent continuum radiative transfer codes (Pascucci et al. 2004).

4.1. *Disk Geometry*

VV Ser is modeled using a density structure consisting of a central disk surrounded by a spherically symmetric envelope. For the central disk, the following density structure is adopted:

$$\rho(R,\ Z) = \frac{\Sigma(R)}{H_p(R)\sqrt{2\pi}} \exp\left[-\frac{Z^2}{2H_p(R)^2}\right], \qquad (1)$$

where $\Sigma(R) = \Sigma_{\rm disk}(R/R_{\rm disk})^{-p}$ is the surface density and

$$H_p(R)/R = (H_{\rm disk}/R_{\rm disk})(R/R_{\rm disk})^{\alpha_{\rm fl}} \qquad (2)$$

is the disk scale height with $\alpha_{\rm fl}$ the flaring index. The flaring index is $\frac{2}{7}$ for a passive irradiated disk with a gray dust opacity (Chiang & Goldreich 1997). For $\alpha_{\rm fl} \lesssim 0$ the disk is nonflaring and shadowed. We have chosen an intermediate value of $\frac{1}{7}$. However, once the disk is self-shadowed, the exact value of the flaring parameter does not have a strong influence on the SED. Equation (1) is appropriate for the vertical structure of an isothermal disk in hydrostatic equilibrium and gives a convinient parameterization, even for disks that are nonisothermal and not in hydrostatic equilibrium.

Indeed, we do not require a vertical structure determined by hydrostatic equilibrium such as that described in Chiang & Goldreich (1997) and Dullemond et al. (2001) but let the outer vertical scale height be a free parameter. While the unique solution of Chiang & Goldreich (1997) assumes that gas and dust are well mixed and thermally coupled, there are several mechanisms that may operate to cause the vertical structure of the dust to deviate significantly from hydrostatic equilibrium. For instance, dust grains may decouple from the gas by grain growth and settling in which case hydrostatic equilibrium no longer applies. Recent modeling of dust settling indicates that it is a rapid process in circumstellar disks and produces highly observable effects (Dullemond & Dominik 2004).

For the structure of the inner disk, we adopt a puffed-up inner rim model similar to that of Dullemond et al. (2001). The scale height of the inner rim, $H_{\rm rim}$, is included as an adjustable parameter. The radius, $R_{\rm rim}$, of the inner rim is set to the location at which a temperature of 1500 K is reached. Note that since the dust in the inner rim does not have a gray opacity, the radius of the inner rim is pushed to a significantly larger radius than that of gray dust. The puffed-up inner rim is connected to the "normal" disk structure by changing the scale height power law of equation (2) at a few times the inner rim radius such that the scale height rises inward to meet the puffed-up inner rim. The radius of the break in the power law is not strongly constrained, and a presumably reasonable value of $2.5 \times R_{\rm in}$ is adopted here.

The disk is surrounded by a large "envelope" simulating the presence of the large-scale molecular cloud. The column density

TABLE 2
ADOPTED DUST COMPONENTS

Component	$a_{\min}$ (μm)	$a_{\max}$ (μm)	Disk Regime
Model 1 (Standard Model) and Model 2			
Small grains	0.005	0.4	$R < 1$ AU, $R > 5000$ AU
Large grains	0.3	3.0	5000 AU $> R >$ 1 AU
Model 3			
Small grains	0.005	0.4	$0.7 < R < 1$ AU, $R > 5000$ AU
Large grains	0.3	3.0	$R < 0.7$, 5000 AU $> R >$ 1 AU

of the cloud is adjusted to reproduce the measured extinction toward VV Ser outside of extinction events. A cavity centered on the star+disk system is carved out of the cloud. Paper II discusses the model fit on large spatial scales, including the detailed structure of the envelope, and how a local model grid for the envelope parameters was calculated, while this paper deals with the parameters of the disk itself.

4.2. *Dust Opacities*

The mid-infrared spectrum and the optical colors indicate that several different dust opacities must be included in the model, corresponding to different parts of the disk. The silicate emission band at 9.7 μm is broader and flatter than an interstellar feature (see § 5.5), indicative of grain growth (Bouwman et al. 2001; Kessler-Silacci et al. 2006), whereas the colors of the flux variations at optical wavelengths indicate that the grains in the innermost parts of the disk are not very different from small interstellar grains. Grains large enough to produce a flat silicate feature will have gray opacities in the optical wave bands. Finally, the PAHs necessary to model the large nebulosity surrounding VV Ser contribute an opacity of their own (see Paper II for details).

The model allows for an arbitrary number of distinct dust reservoirs with relative abundances that may vary throughout the grid. In the VV Ser disk, we use two distinct dust components: The first consists of small grains that produce non-gray opacities in the optical wave bands, the second component consists of larger $\sim$1 μm grains. The small-grain dust is located in the puffed-up rim ($\lesssim$1 AU), while the rest of the disk is populated with the larger grain component.

The opacities of the thermalized dust grains are calculated using Mie theory. The grains are spherical silicates with inclusions of carbonaceous material. The silicate optical constants are those of oxygen-rich silicates from Ossenkopf & Henning (1994), while the carbon optical constants are of carbon clusters formed at 800 K from Jäger et al. (1998). We do not include any ice component in the dust opacity. The Maxwell-Garnett effective medium formula (e.g., Bohren & Huffman 1983) has been used to calculate the optical constants of the silicate with carbon inclusions. The volume fraction of the carbon is 30%, roughly consistent with that determined by Draine (2003). The final opacities are then calculated with a grain size distribution consisting of a power law: $dN(a)/da \propto a^{-3.5}$ with minimal ($a_{\min}$) and maximal ($a_{\max}$) grain sizes. The disk SED is attenuated by foreground dust from an extended envelope, which is discussed in detail in Paper II. The exact choices of grain size distributions for the disk dust are justified in § 5.4 (optical colors) and § 5.5 (silicate emission feature), and the dust parameters are summarized in Table 2. For comparison to other dust opacities, it is useful to note that the "large grain" dust opacity of the disk has $\kappa_{850\mu m} = 0.01$ cm^2 g^{-1} $\times$ ($R_{\text{gas to dust}}$/100), where $R_{\text{gas to dust}}$ is the gas to dust ratio. This is similar to, but on the small side of the opacities (for coagulated grains) of Ossenkopf & Henning (1994).

5. OBSERVED FEATURES EXPLAINED BY THE MODEL

5.1. *Constraining the Model*

Due to the long computing times for a single model, the model parameters are varied by hand. Rather than calculating a comprehensive grid in all parameters, hundreds of models were calculated until a good fit was found to all the observable quantities. While this is not an optimal method for quantifying any degeneracies in the fit, some parameters may be independently constrained on physical grounds. In Table 3, the parameters of the best-fitting model are summarized. This model has been constructed using all available observational constraints apart from the near-infrared interferometry visibilities discussed in § 5.6. We refer to this model as "model 1." The density and temperature structure of model 1 are shown in Figure 1. The SED of model 1 is compared to the observed SED of VV Ser in Figure 2. In §§ 5.2–5.5, we discuss how each observation property is connected to the model. In § 5.6 it is discussed how the near-infrared interferometry from the literature requires model 1 to be modified on small scales.

5.2. *Extinction Events*

The optical light curve of VV Ser, observed by Rostopchina et al. (2001) is shown in Figure 3. It is seen that the light curve of VV Ser contains a number of extinction events, each lasting a few days. Although each event is undersampled, their average

TABLE 3
BEST-FITTING MODEL PARAMETERS

Parameter	Model 1	Model 2	Model 3	Estimated range (see text)
Luminosity ($L_\odot$)	49	...	...	45–55
Spectral type	B9 (10,200 K)	...	...	A2–B6
Dust mass ($M_\odot$)	0.8×10^{-7}	...	...	$0.1–8.0 \times 10^{-7}$
p	-1	...	...	Not explored
α_{fl}	1/7	...	...	Not explored
$H_{\text{disk}}/R_{\text{disk}}$	0.125	...	...	0.1–0.15
$H_{\text{rim}}/R_{\text{rim}}$	0.105	...	...	0.1–0.15
T_{sub} (K)	1500	2000	1500	1300–1600
R_{rim} (AU)	0.7	0.4	0.27 and 0.80	Given by T_{sub}
R_{disk} (AU)	50	...	...	20–200
Inclination (deg)	71.5	40	68	65–75
P.A. (deg)	11	170	15	10–20 (see Paper II)

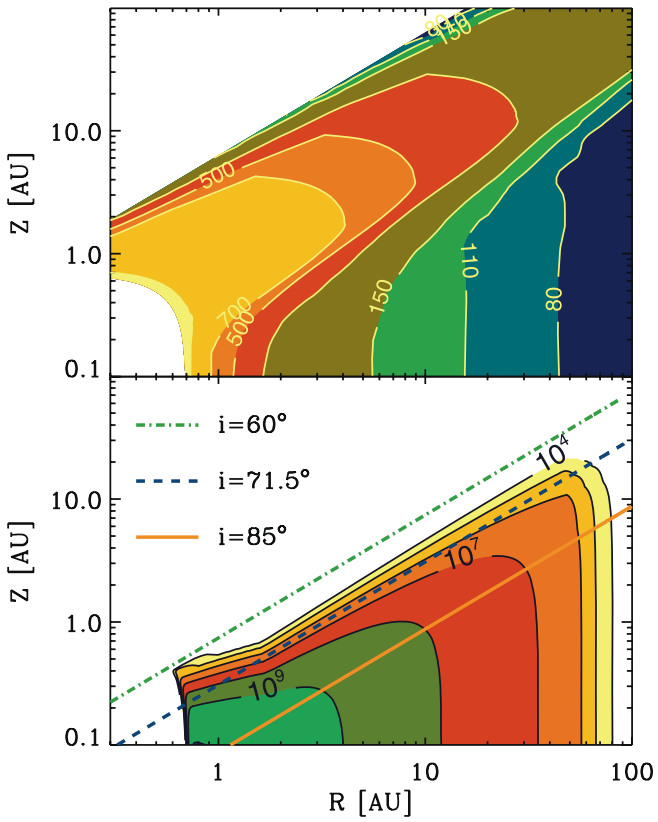

FIG. 1.—Physical structure of the disk model. *Top*: Temperature of the disk as calculated by RADMC in kelvins. *Bottom*: Density structure of the disk in units of hydrogen molecules per cubic centimeter. The three lines indicate the path from the central star to an observer for different inclination angles. Note that for the best-fitting inclination angle of 71.5°, the line of sight to the central star passes through both the puffed-up inner rim as well as part of the outer disk.

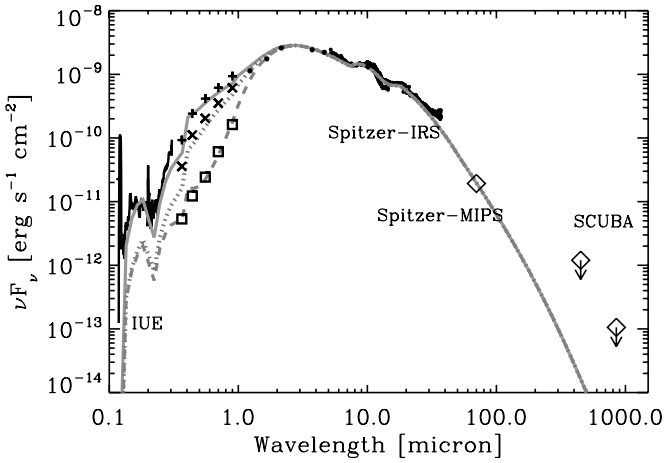

FIG. 2.—Observed SED of VV Ser compared to SEDs of model 1. The three model SED curves correspond to a varying optical depth of the perturbation of the inner rim responsible for the observed UX Ori extinction events (*solid curve*: corresponds to $\Delta A_V = 0$ mag; *dotted curve*: $\Delta A_V = 0.75$ mag; *dashed curve*: $\Delta A_V = 4.0$ mag). The sets of optical data corresponding to the symbols (*plus signs*, *times crosses*, and *open squares*) are single points in the light curve obtained. [*See the electronic edition of the Journal for a color version of this figure.*]

duration can be estimated by searching for the duration most compatible with all the observed events. Assuming that the extinction events have an identical Gaussian shape in the light curve and vary only in intensity, it is found that the events are consistently shorter than 5.5 days and longer than 3.0 days (FWHM). The best-fitting Gaussian is shown in the right panel of Figure 3. The width of any perturbation of the inner rim causing an extinction event is likely to be less than or comparable to the pressure scale height of the disk. Scenarios in which this is not the case are interesting to consider but probably require hydrodynamical simulations to constrain. Assuming Keplerian rotation, this requirement constrains the radius of the inner rim of the disk, since a rim radius that is too small will cause extinction events to be shorter than those observed. An inner radius corresponding to a dust sublimation temperature of 1500 K for small grains is located at 0.7–0.8 AU at the VV Ser luminosity of $\sim$49 $L_\odot$. This corresponds to a rotation period of the inner rim of $\sim$180 days and a physical size of the dust perturbation causing the extinction in the azimuthal direction of 0.09–0.15 AU. A spherical dust perturbation then has an average density of 2–3 $\times$ 10^9 cm^{-3} in order to produce a maximum observed extinction of 5 mag in the V band. These values are close to those of the model with an inner rim scale height of $H_{\rm rim}/R_{\rm rim} = 0.105$ and a maximum gas density along the line of sight of $\sim 10^9$ cm^{-3} between extinction events for an inclination of $\sim$70°. A specific extinction event then corresponds to creating an overdensity in the inner rim enhanced by a factor of a few compared to the "quiescent" state of the inner disk.

5.3. *The Outer Radius*

The outer radius of the disk is not well constrained and is somewhat degenerate with the disk opening angle. The mass is constrained by the 70 μm MIPS point and the 850 μm upper limit to be as low as $8 \times 10^{-6} \times (R_{\rm gas\ to\ dust}/100)\ M_\odot$. As usual, it must be stressed that the observations do not probe grains that have grown to sizes of more than a few millimeters, and the disk may contain a significant population of such grains in the midplane. Similarly, any total mass estimate will necessarily assume a dust-to-gas ratio of 100, but this is likely to be very different for a disk as evolved as VV Ser. The mass of small dust grains is accurate to the uncertainty in the far-infrared opacity, i.e., by a factor of a few.

5.4. *Optical Photometry and Variability*

As discussed in § 4.2, the observation that the grains responsible for the silicate emission features appear to be different from those responsible for the extinction events is taken into account in the model. While many UX Orionis stars appear to have disks in which the dust causing the extinction events is dominated by small grains ($a \lesssim 1$ μm; van den Ancker 1999), models of grain growth predict that the inner parts of disks very quickly become dominated by large grains (Dullemond & Dominik 2005). A priori, it is not clear why the grains responsible for the extinction events have a different size distribution than those of the outer disk. As a first attempt, we simply model the observations by changing the opacity of the dust in the puffed-up inner rim at radii between the rim and the break in the scale height power law defined in § 4 (see Table 2). This has the effect of converting the gray (in the UV–NIR) disk opacity to one reproducing the optical colors. Note that this also causes the inner rim to absorb visible photons more efficiently than it reemits the energy in the near-infrared. This significantly increases the temperature of the star-facing surface of the rim and has the effect of pushing the rim outward, given a certain dust sublimation temperature. Possible alternative geometries are discussed in § 5.6.

The grain model of the material causing the extinction events is constrained by the optical extinction curve that can be derived by the observed optical reddening vectors. The extinction events correspond to grains that appear to have properties similar to those

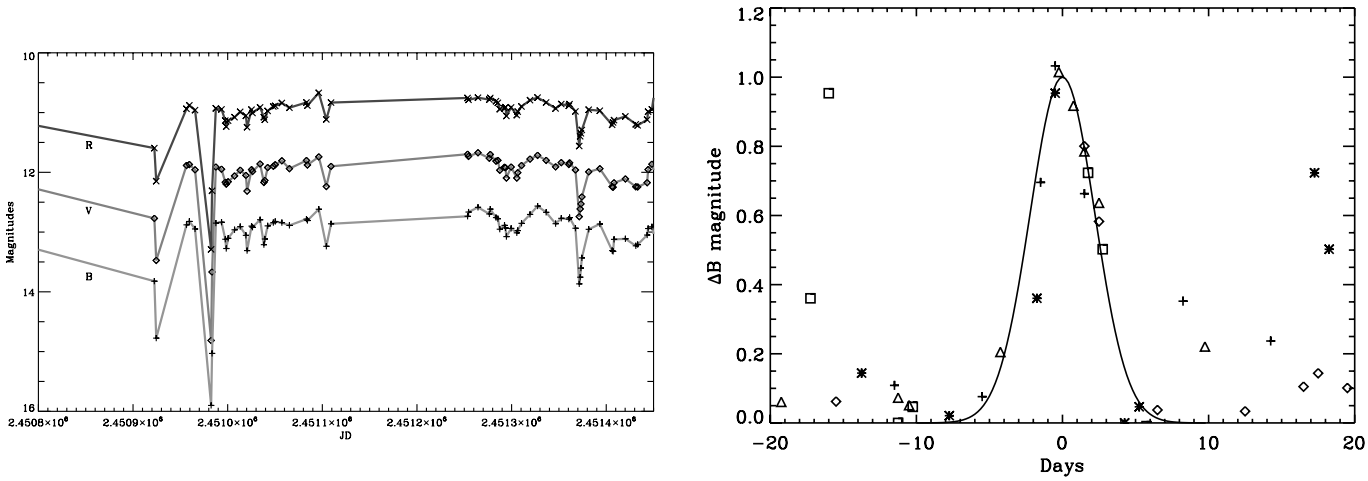

FIG. 3.—*Left*: Optical light curve of VV Ser from the catalog of Rostopchina et al. (2001) spanning the best-sampled 2 years. *Right*: Average profile of the extinction events over the best-sampled 2 year period. The curve is a Gaussian with a FWHM of 5.5 days. [*See the electronic edition of the Journal for a color version of this figure.*]

of interstellar grains. The reddening vectors in the optical color-magnitude diagrams are fitted by a power-law grain size distribution by varying the minimum and maximum sizes as well as the power-law index. Not unexpectedly, a good fit is found for $a_{\rm min} = 0.05\ \mu$m and $a_{\rm max} = 0.4\ \mu$m, giving an optical extinction law with $R_V \sim 3.6$.

As discussed in § 5.1 the perturbations of the inner rim are presumably not wider in the azimuthal direction than the pressure scale height. In essence this means that a dust perturbation in a Keplerian orbit roughly subtending 10°, as seen from the star, is responsible for an extinction event. The optical variability of VV Ser is therefore fundamentally a three-dimensional effect and to model it within the axisymmetric framework presented here requires some assumptions. If it is assumed that the azimuthal angle the dust perturbation subtends as seen from the star is $\ll 2\pi$ and that the shadowing and scattering effects caused by the perturbation will not affect the thermal part of the SED. In this case only the extinction at a specific inclination through the perturbation needs to be taken into account. This means that the temperature structure of the system can be calculated for the "quiescent" state of the inner rim in which no localized perturbation of dust is providing extra extinction toward the star. The "active" state corresponding to an extinction event is simulated by using the temperature structure calculated by the Monte Carlo code, but adding extra extinction to the input spectrum of the central star when calculating the final SED by ray-tracing. Thus, by attenuating the star by a variable amount of dust, model tracks through the optical color-magnitude diagrams can be constructed and compared to the observed tracks. The effect on the SED of attenuating the input stellar spectrum by a variable extinction (ΔA_V) is shown in Figure 2 and compared to photometric data obtained during and outside of extinction events.

In the model for VV Ser, a blueing effect occurs naturally because scattering dominates the optical flux for high optical depths through the extincting blob of dust. The resulting model tracks are plotted on the observed photometric points for VV Ser in Figure 4. The tracks correspond to A_V values of 0.0–4.0 mag. It is seen that a strong blueing effect appears for $A_V \gtrsim 2.5$ mag. The blueing is

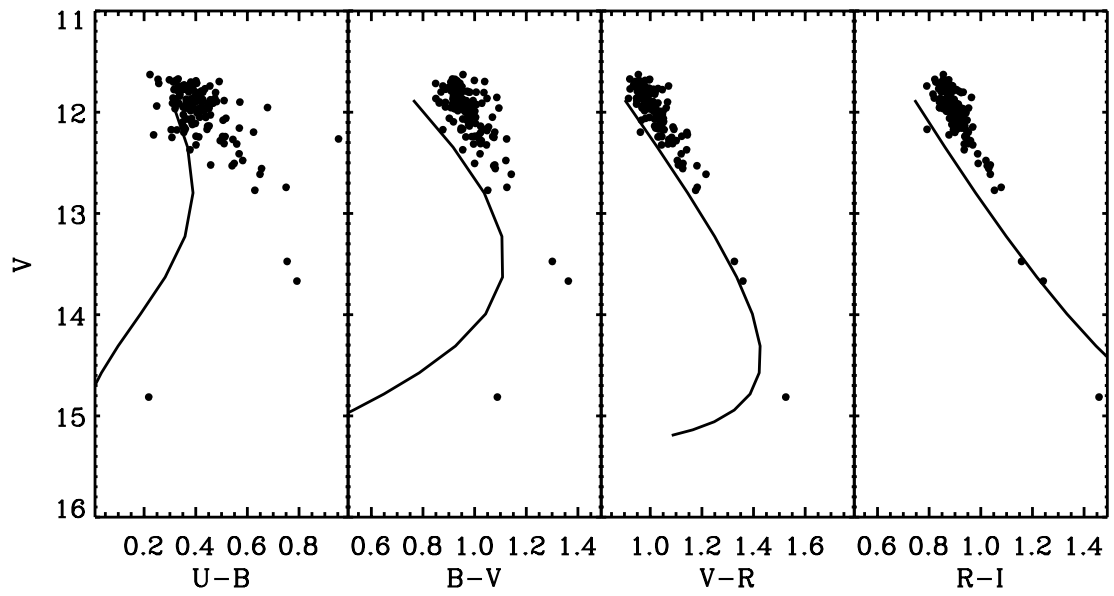

FIG. 4.—Color-magnitude diagrams of the photometry of VV Ser from Rostopchina et al. (2001) compared to curves calculated using the radiative transfer model. The model curves correspond to extinction events of $A_V = 0$–4 mag. The small 0.15 mag offset in the $R - I$ color is due to an inaccuracy in either to model photospheric color or the inner rim color.

strongest in the $B - V$ color. In $R - I$ a slight reddening is seen instead. This is due to the I-band photons being slightly dominated by thermal emission from the 1500 K inner rim rather than from scattering of photospheric photons. The model approximately reproduces this behavior, although some differences are noticeable. The use of isotropic scattering, as opposed to nonisotropic scattering that tends to be forward throwing, may account for some (up to a factor of 2 in absolute flux) of this difference. There are also slight absolute offsets between the model colors and the observed colors. This offset may be due to inaccuracies in the stellar spectrum. The differences in colors between the possible range of spectral types (A2 to B6; see Table 3) is 0.55, 0.20, 0.14, and 0.12 mag for $U - B$, $B - V$, $V - R$, and $R - I$, respectively, differences similar to or larger than the model-data offsets. Finally, small changes in the Johnson filter curves used in the models can produce similar offsets.

5.5. *Mid-Infrared Spectrum*

The 5.2–37.0 μm spectrum as observed by the *Spitzer* IRS is dominated by the silicate emission bands at 9.7 and 18 μm. The 9.7 μm band is significantly broader and flatter than that of interstellar silicate grains. This is illustrated in Figure 5 where the shapes of the observed silicate bands are compared to those of dust opacities corresponding to grains of different sizes. In the figure, the disk continuum has been subracted by fitting a power law to the spectrum at 5.5, 13, and 30–40 μm, following the procedure of Kessler-Silacci et al. (2006). A broadening of the 9.7 μm silicate band is indicative of a grain size distribution dominated by grains larger than $\sim$1 μm (van Boekel et al. 2005; Kessler-Silacci et al. 2006). Other emission features may appear to broaden the silicate bands. These include emission bands due to PAHs that in the case of VV Ser are visible at 6.2 μm and possibly at 11.3 μm, although this feature may also be due to crystalline silicates (see also Geers et al. 2006). Because they are bright and unresolved, the PAH emission features are not related to the larger nebulosity discussed in Paper II and are most likely due to material associated with the disk. The exact dust size distribution of the "large grain" component is not strongly constrained by the silicate features, in particular not in the disk midplane. Here, we adopt a dust mixture with diameters $a_{\rm min} = 0.3$ μm and $a_{\rm max} = 3.0$ μm. The most important property of the large grain mixture, for the purposes of this model, is that it has gray optical and near-infrared opacities. As long as this condition is satisfied, the conclusions reached from the modeling are not sensitive to the details in the size distribution of the large grain component. It is likely that the dust mass of the disk has a significant population of much larger (millimeter-sized) grains (e.g., Dullemond & Dominik 2005), but this component is not constrained by the observations presented here.

Another parameter constrained by the *Spitzer* IRS spectrum, central to the discussion of VV Ser as a UX Orionis class Herbig Ae star, is the slope of the mid-infrared SED. As suggested by Dullemond et al. (2003) if the innermost regions of the disk are responsible for the extinction events, the outer disk must have a scale height, H/R, similar to or smaller than that of the puffed-up inner rim. This is the definition of a self-shadowed disk, characterized by a declining spectrum for $\lambda > 5$ μm with weak silicate emission features. This type of object also corresponds to a "group II" object in the classification of Meeus et al. (2001). VV Ser clearly has a mid-infrared SED that suggests that the disk is self-shadowed. However, in the model, the declining SED is in part caused by the low mass of the disk, i.e., to avoid predicting too much flux at $\lambda > 5$ μm, the models are constrained both to be self-shadowed and to have a total gas+dust mass of $M \lesssim 10^{-5}$ $M_\odot$. In particular, the low mass is necessary to keep the SED declining beyond $\sim$30 μm, while the shadow of the puffed-inner rim ensures that the SED declines between 5 and 30 μm. A simple test of this was conducted by removing the puffed-up inner rim from the model, which resulted in a flat SED below 30 μm. In the best-fitting model, 90% (1.3 mag) of the extinction at 0.2 μm in the disk along a sight line inclined at 71.5° relative to the disk axis occurs within 1.5 AU.

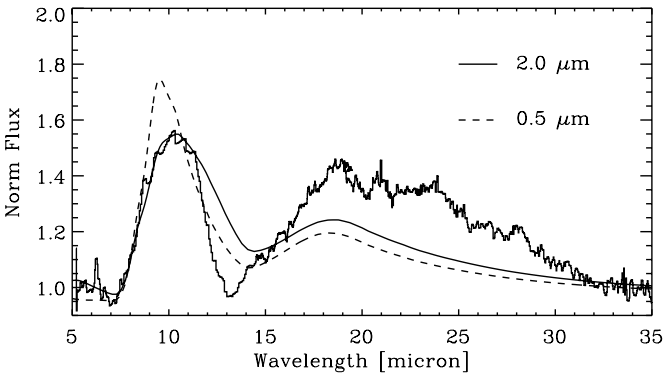

FIG. 5.—*Spitzer* spectrum of the silicate emission features of VV Ser compared to opacities of spherical grains with diameters of 1.0 and 3.0 μm. A power-law continuum has been subtracted from both the observed spectrum as well the opacity.

Does the model suggest that the scale height of the disk has been lowered due to dust settling, or has only the apparent dust mass been lowered? The scale height, H_p/R for hydrostatic equilibrium at 50 AU is 0.09. This is somewhat smaller than the model scale height of 0.12. However, this value is not strongly constrained, as long as the inner disk shadows the outer, it is difficult to tell the difference without having more sensitive photometry at wavelengths longer than 70 μm.

5.6. *Near-Infrared Interferometry*

Several interferometric measurements of the near-infrared morphology of the innermost part of the VV Ser system are available in the literature. Eisner et al. (2003, 2004) presented K-band interferometry observations of VV Ser performed with the Palomar test bed interferometer. These authors find a K-band size of VV Ser of $\sim$3 mas for a generic flared disk with a puffed-up inner rim from Dullemond et al. (2001). This corresponds to $R_{\rm rim} \sim 0.39 \times (d/260\ {\rm pc})$ AU, or exactly half of the radius used in model 1. In principle, this smaller radius will result in a dust temperature in the inner rim of $\sim$2000 K, using the opacity stipulated by the extinction events. While the interferometry does suffer from a poor sampling of the u-v plane, this is a discrepancy which deserves a closer look. There are several ways of resolving the problem: the presented model includes a large cleared-out inner region due to the high temperatures of small grains. However, the location of the rim, given a dust sublimation temperature, actually depends on the dust opacity. A nongray opacity will tend to absorb more energy in the optical than it can emit in the near-infrared, increasing the temperature of the grains in the optically thin region of the puffed-up inner rim. This will tend to erode the inner edge of the rim, as small grains are heated above their sublimation temperature. This is reflected in the inner radius of model 1. Conversely, larger grains with a more gray opacity will significantly decrease the temperature at a given radius of the inner rim, and consequently $R_{\rm rim}$ will decrease for the same dust sublimation temperature. Specifically, using the grain opacity for the outer (>2 AU) disk rather than the grains responsible for the

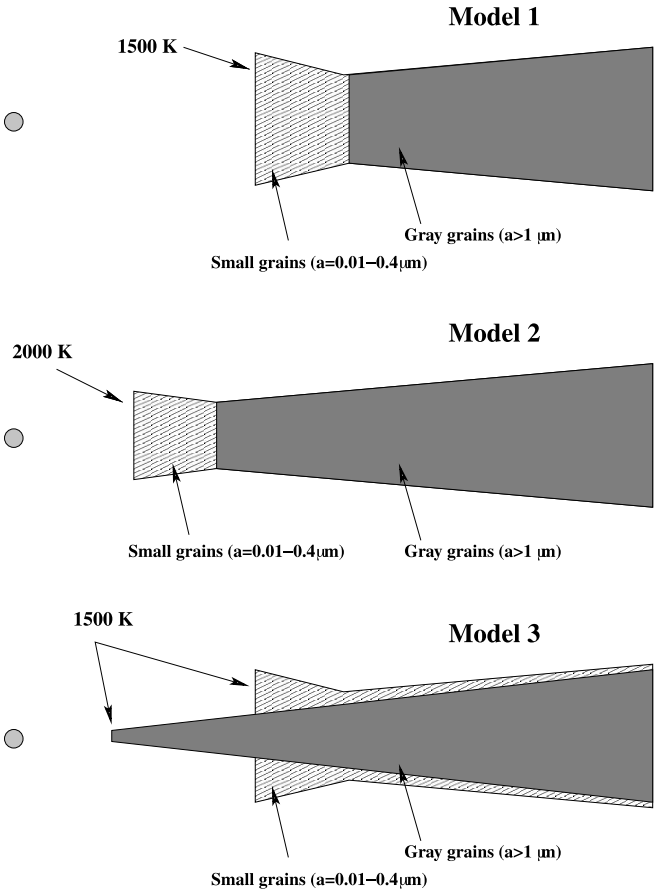

FIG. 6.—Sketches showing the inner rim structure for three different disk models that have been compared to the interferometry and SED. *Top*: "Standard" model with the inner rim consisting of small grains at 1500 K, placing it at 0.8 AU. This model fits the SED, but not the visibilities. *Middle*: Model using the inner rim radius of ~0.4 AU suggested by Eisner et al. (2004). Using the inclination and position angle from Paper II as well as small grains in the rim, this model fits neither SED nor visibilities. The visibilities can be fit better by changing the position angle and inclination significantly. *Bottom*: Model using an inner rim at 1500 K for both grains populations present in the disk (small and gray grains). This model fits both the SED and visibilities with the position angle and inclination from Paper II. [*See the electronic edition of the Journal for a color version of this figure.*]

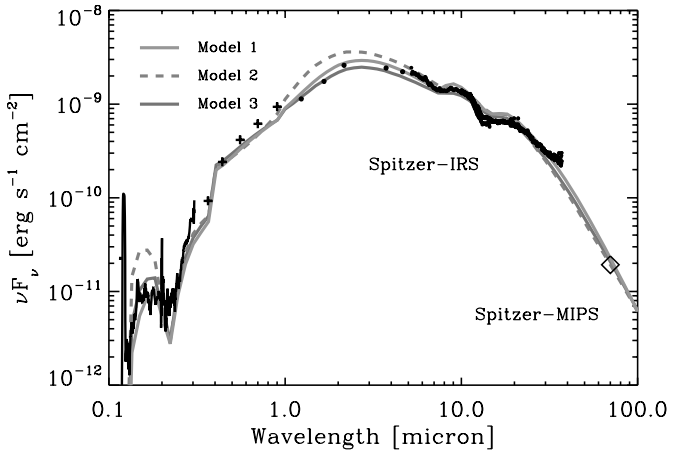

FIG. 7.—Spectral energy distributions for VV Ser using three different models for the inner rim (see Fig. 6 and Table 3). [*See the electronic edition of the Journal for a color version of this figure.*]

UX Orionis events, will place the inner rim close to the value determined by Eisner et al. (2004), i.e., 0.3–0.4 AU for an optically thick inner rim. This scenario then requires that small grains only appear in the upper layers of the puffed-up rim, while larger grains can penetrate close to the star in a flatter structure. This extra component of large grains within the present inner rim does not strongly affect the model SED of VV Ser.

To explore the possibilities offered by interferometry, we have calculated the visibilities for our model, as well as several alternative structures of the inner rim, and compared them to those from Eisner et al. (2004). In Figure 6 the structures of three different types of inner rim are sketched (model 1 refers to the standard model discussed in the previous sections). Figure 7 shows the calculated SEDs for the three models, while Figure 8 shows the best-fit visibilities from the three models (allowing the position and inclination angles to vary). In the following, position angles are those of the disk plane measured east of north. It is clear that given the position angle derived from the *Spitzer* images presented in Paper II, the north-west baseline visibilites can be well fitted, but the north-south and south-west baselines produce visibilities that are severely underpredicted by model 1, i.e., the visibilities are overresolved in the direction of the disk plane. As noted by Eisner et al. (2004) the single point observed with the south-west baseline may be significantly more uncertain than the statistical error bar indicates. We therefore assign little weight to this point. However, the bad fit to the north-south baseline appears significant. Given the sparse *uv* coverage, several widely different scenarios may provide better fits.

First, assuming that the position angle of 10°–20° from Paper II is correct, the easiest way to amend the model to fit the near-infrared visibilities is by making the radius of the inner rim significantly smaller, thereby increasing the visibility along the major axis of the system. *K*-band visibilities of a model in which the inner rim radius has artificially been placed at 0.4 AU has been calculated (model 2 in Fig. 6). A significant problem with this model is that it does not fit the SED because the small grains in the inner rim reach temperatures of 2000 K. Note that Eisner et al. (2004) finds a temperature of 1500 K at this radius due to an assumption of a gray opacity for the inner rim. In addition, a good fit to all three baselines can only be found for a position angle of ~165° and an inclination of 40°, consistent with the findings of Eisner et al. (2004) but inconsistent with the orientation of the surrounding nebulosity as described in Paper II. Recently, Isella et al. (2006) found a position angle of 60°–120° using the same interferometric data, roughly consistent with the result of Eisner et al. (2004). If the single uncertain point of the south-west baseline is ignored, a good fit can be found for the ~70° inclination and ~10° position angle found in Paper II. These two possibilities need to be tested by further interferometric observations.

Another option to reconcile the interferometry with the *Spitzer* images is a model in which large grains in the disk midplane reach smaller radii in an optically thin region within the outer puffed-up inner rim (model 3 in Fig. 6). This structure is, in fact, quite plausible since the temperature can be maintained below 1500 K, as discussed above. This is presumably a natural scenario in a disk in which the large grains have settled to the midplane. We therefore construct a model in which the structure of the "standard" model is maintained (with small grains in a puffed-up inner rim), but with an additional component between 0.27 and 0.8 AU consisting of the large grains of the outer disk and with a structure following equation (2). Essentially, this model represents a rough simulation of the effect of grain settling and density-dependent evaporation on the structure of the inner rim. This disk has basically two rims, both with a maximum dust temperature of 1500 K. The central idea of this scenario is that the SED is not strongly affected, since both dust components have a temperature of ~1500 K. At the same time, the visibilities can be fitted by a

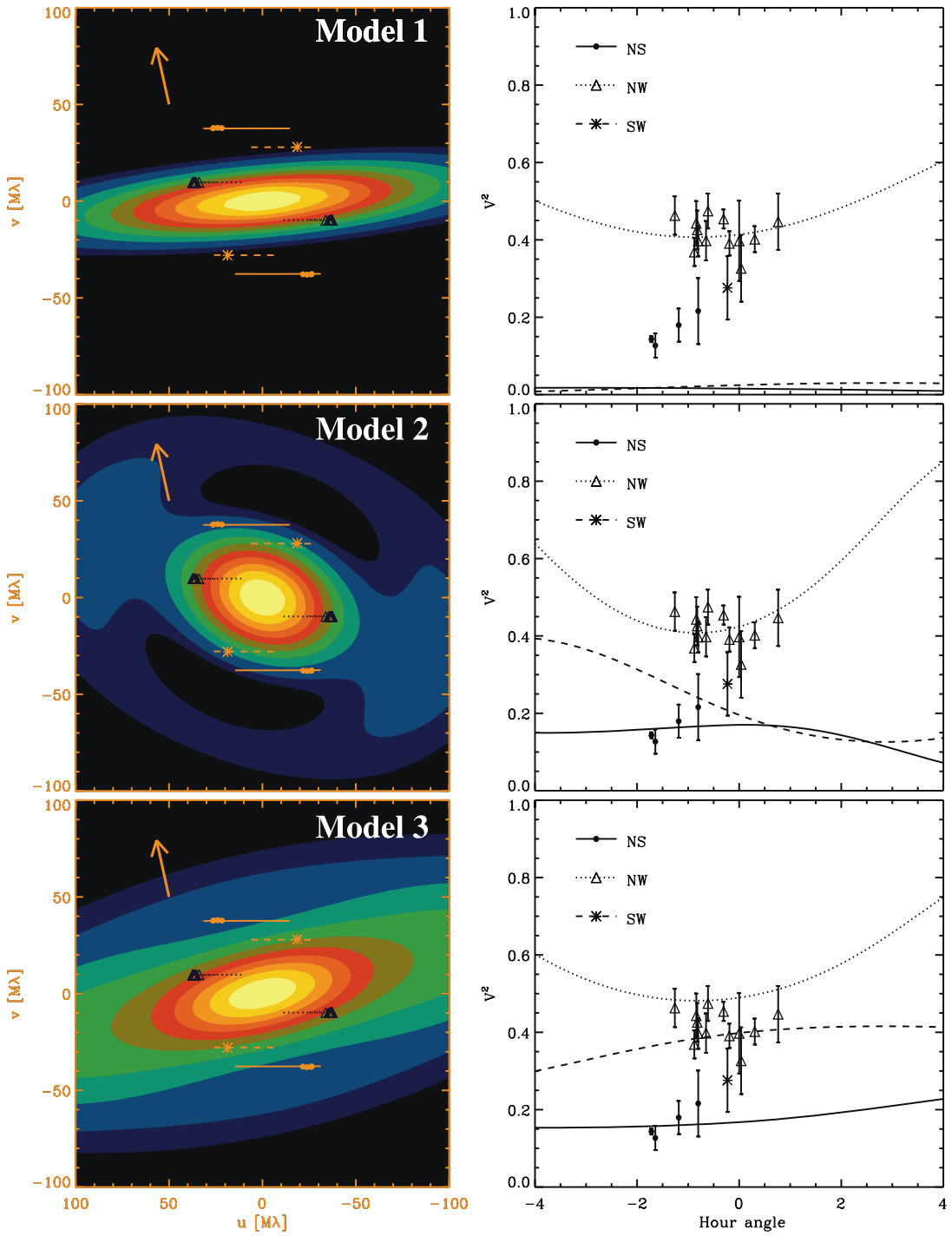

FIG. 8.—Normalized *K*-band visibility amplitudes of the of the "standard" model (model 1), the model with an inner rim at 0.4 AU (model 2) and the model simulating settling of larger grains to the disk midplane (model 3). The observed visibilities are from Eisner et al. (2004). The positition angle has been varied to find the best fit within −30° and 30°. The range was chosen to be reasonably consistent with the orientation of the bipolar nebulosity around VV Ser presented in Paper II. The arrow indicates the position angle of the disk plane suggested by the *Spitzer* images presented in Paper II (13°). The symbols indicate the observed *uv* points for the three baselines, while the curves show the model tracks (*left*) and visibilities as a function of hour angle (*right*).

disk with the same position angle and inclination as that found in Paper II using the morphology of the nebulosity seen in the IRAC and MIPS images of VV Ser. By tweaking additional parameters such as the density structure of the gray dust and the exact location of the inner rim, an excellent fit to all the observables can be obtained. In particular, we find that a better fit to the visibilities is achieved if the surface density within 0.8 AU is lowered by a factor of 5 to create an inner large grain component with roughly unity optical depth in the radial direction. This creates an inner rim that is not perfectly sharp, but radiates at a range of radii. This seems consistent with the structure predicted by Isella & Natta (2005) using a density dependent grain evaporation temperature.

Another option to fit the interferometer data is to add an additional point source offset by a few milliarcseconds to produce

additional visibility in the north-west and south-west baselines. We do not attempt to model this scenario here, but simply note that a few extra visibility data points will be able to distinguish between an additional point source and a small inner rim.

Finally, it is possible that hot gas within the inner rim may produce a significant contribution to the *K*-band continuum as suggested by Akeson et al. (2005) who showed models of Palomar Testbed Interferometer (PTI) visibilities for a small sample of T Tauri stars. In fact, gas may produce much the same near-infrared morphology as that modeled here using two dust components. However, in order for the gas to be sufficiently luminous, a high accretion rate of at least $10^{-7}\ M_{\odot}\ \mathrm{yr}^{-1}$ is required (Muzerolle et al. 2004). The accretion rate of VV Ser is lower than this, as evidenced by the lack of UV excess and the very low disk mass.

6. CONCLUSIONS

We have presented *Spitzer* mid-infrared spectroscopy of the UX Orionis star VV Ser combined with additional spectroscopy and imaging data from the literature spanning wavelengths from 0.1 to 850 μm. Using an axisymmetric dust radiative transfer model, we have reached the following conclusions:

1. All available data are consistent with the interpretation of the UX Orionis phenomenon in which the central star is transiently attenuated by dust clumps in the inner puffed-up region of an inclined, self-shadowed disk (the specific inclination is supported by the imaging data presented in Paper II). While VV Ser is a very specific case that has been singled out due to the availability of a wealth of multiwavelength, high-quality data, it provides strong support for this interpretation in the more general case.

2. The disk appears to be both self-shadowed and low mass, and both properties contribute to the quick decline with wavelength of the SED at mid- and far-infrared wavelengths.

3. The duration of the extinction events is consistent with an orbit of the dust perturbations in the inner rim at a radius of $\sim$1 AU.

4. The dust responsible for the extinction events must be dominated by small, interstellar-like grains, while the dust in the outer (>2 AU) disk appears to be dominated by somewhat larger grains ($\sim$1 μm). It is unlikely that the extincting dust clumps can be located significantly closer to the central star, since this would require them to subtend a much larger azimuthal angle than that corresponding to the scale height of the inner rim. In addition, they would be heated above their sublimation temperature.

5. Our best-fit inner rim radius of 0.8 AU is in contradiction with the *K*-band interferometry of Eisner et al. (2004), which clearly indicates an inner rim radius of 0.3–0.4 AU. A possible solution is to let the puffed-up inner rim consist of small grains at 0.8 AU while allowing a population consisting of larger grains to penetrate to 0.25 AU in a midplane that is optically thin to infrared photons.

6. The detailed structure of the inner rim described above is constrained *both* from the interferometry *and* the independent measurement of the disk inclination and position angles from large scale imaging as discussed in Paper II.

7. We therefore interpret the *K*-band interferometric data of Eisner et al. (2004) as evidence for larger grains in the disk midplane penetrating closer to the star than the small grains in the puffed-up inner rim. This is consistent with a scenario in which all dust grains sublimate at $\sim$1500 K and larger grains have settled to the disk midplane, leaving only small grains in the disk surface.

8. Clearly, further tests of the detailed structure of the puffed-up inner rim are within reach of the current observational capabilities. Aperture synthesis observations with upcoming facilities such as the Very Large Telescope Interferometer (VLTI) AMBER instrument, in combination with multiwavelength imaging and spectroscopy, are certain to greatly enhance our understanding of the innermost parts of protoplanetary disks.

The authors are grateful to Josh Eisner for providing a table with the PTI visibilities of VV Ser and Remo Tilanus for obtaining the SCUBA map in service mode. Support for this work was provided by NASA through Hubble Fellowship grant 01201.01, awarded by the Space Telescope Science Institute, which is operated by AURA, Inc., for NASA, under contract NAS5-26555. Astrochemistry in Leiden is supported by a Spinoza grant of the Netherlands Organization for Scientific Research (NWO). Support for this work, part of the *Spitzer Space Telescope* Legacy Science Program, was provided by NASA through contracts 1224608 and 1230779, issued by the Jet Propulsion Laboratory, California Institute of Technology, under NASA contract 1407. This research was supported by the European Research Training Network The Origin of Planetary Systems (PLANETS, contract HPRN-CT-2002-00308). The anonymous referee is thanked for constructive comments that have significantly improved the paper.

REFERENCES

Akeson, R. L., et al. 2005, ApJ, 622, 440
Berrilli, F., Corciulo, G., Ingrosso, G., Lorenzetti, D., Nisini, B., & Strafella, F. 1992, ApJ, 398, 254
Bertout, C. 2000, A&A, 363, 984
Bohren, C. F., & Huffman, D. R. 1983, Absorption and Scattering of Light by Small Particles (New York: Wiley)
Bouwman, J., Meeus, G., de Koter, A., Hony, S., Dominik, C., & Waters, L. B. F. M. 2001, A&A, 375, 950
Chiang, E. I., & Goldreich, P. 1997, ApJ, 490, 368
Draine, B. T. 2003, ARA&A, 41, 241
Duchêne, G., Ménard, F., Stapelfeldt, K., & Duvert, G. 2003, A&A, 400, 559
Dullemond, C. P., & Dominik, C. 2004, A&A, 417, 159
———. 2005, A&A, 434, 971
Dullemond, C. P., Dominik, C., & Natta, A. 2001, ApJ, 560, 957
Dullemond, C. P., & Turolla, R. 2000, A&A, 360, 1187
Dullemond, C. P., van den Ancker, M. E., Acke, B., & van Boekel, R. 2003, ApJ, 594, L47
Eisner, J. A., Lane, B. F., Akeson, R. L., Hillenbrand, L. A., & Sargent, A. I. 2003, ApJ, 588, 360
Eisner, J. A., Lane, B. F., Hillenbrand, L. A., Akeson, R. L., & Sargent, A. I. 2004, ApJ, 613, 1049
Evans, N. J., et al. 2003, PASP, 115, 965
Grady, C. A., Sitko, M. L., Bjorkman, K. S., Perez, M. R., Lynch, D. K., Russell, R. W., & Hanner, M. S. 1997, ApJ, 483, 449
Geers, V. C., et al. 2006, A&A, 459, 545
Grinin, V. P. 1988, AZh Pis'ma, 14, 65
Hernández, J., Calvet, N., Briceño, C., Hartmann, L., & Berlind, P. 2004, AJ, 127, 1682
Houck, J. R., et al. 2004, ApJS, 154, 18
Isella, A., & Natta, A. 2005, A&A, 438, 899
Isella, A., Testi, L., & Natta, A. 2006, A&A, 451, 951
Jäger, C., Mutschke, H., & Henning, T. 1998, A&A, 332, 291
Kenyon, S. J., Calvet, N., & Hartmann, L. 1993, ApJ, 414, 676
Kessler-Silacci, J., et al. 2006, ApJ, 639, 275
Meeus, G., Waters, L. B. F. M., Bouwman, J., van den Ancker, M. E., Waelkens, C., & Malfait, K. 2001, A&A, 365, 476
Meijerink, R., Tilanus, R. P. J., Dullemond, C. P., Israel, F. P., & van der Werf, P. P. 2005, A&A, 430, 427
Mora, A., et al. 2001, A&A, 378, 116
Muzerolle, J., D'Alessio, P., Calvet, N., & Hartmann, L. 2004, ApJ, 617, 406
Natta, A., Prusti, T., Neri, R., Wooden, D., Grinin, V. P., & Mannings, V. 2001, A&A, 371, 186

Natta, A., & Whitney, B. A. 2000, A&A, 364, 633
Ossenkopf, V., & Henning, T. 1994, A&A, 291, 943
Pascucci, I., Wolf, S., Steinacker, J., Dullemond, C. P., Henning, T., Niccolini, G., Woitke, P., & Lopez, B. 2004, A&A, 417, 793
Pontoppidan, K. M., & Dullemond, C. P. 2005, A&A, 435, 611
Pontoppidan, K. M., Dullemond, C. P., Blake, G. A., Evans, N. J., II, Geers, V. C., Harvey, P. M., & Spiesman, W. 2007, ApJ, 656, 991 (Paper II)
Pontoppidan, K. M., Dullemond, C. P., van Dishoeck, E. F., Blake, G. A., Boogert, A. C. A., Evans, N. J., II, Kessler-Silacci, J. E., & Lahuis, F. 2005, ApJ, 622, 463
Rostopchina, A. N., Grinin, V. P., & Shakhovskoi, D. N. 2001, Astron. Rep., 45, 51
Siess, L., Dufour, E., & Forestini, M. 2000, A&A, 358, 593
Straizys, V., Cernis, K., & Bartasiute, S. 1996, Baltic Astron., 5, 125
Thi, W. F., Pontoppidan, K. M., van Dishoeck, E. F., Dartois, E., & d'Hendecourt, L. 2002, A&A, 394, L27
van Bemmel, I. M., & Dullemond, C. P. 2003, A&A, 404, 1
van Boekel, R., Min, M., Waters, L. B. F. M., de Koter, A., Dominik, C., van den Ancker, M. E., & Bouwman, J. 2005, A&A, 437, 189
van den Ancker, M. 1999, Ph.D. thesis, Univ. Amsterdam
Watson, A. M., & Stapelfeldt, K. R. 2004, ApJ, 602, 860
Werner, M. W., et al. 2004, ApJS, 154, 1
Wolf, S., Padgett, D. L., & Stapelfeldt, K. R. 2003, ApJ, 588, 373
Wood, K., Wolff, M. J., Bjorkman, J. E., & Whitney, B. 2002, ApJ, 564, 887